Vast CO2 release from Australian fires in 2019–2020 constrained by satellite

van der Velde, Ivar R.; van der Werf, Guido R.; Houweling, Sander; Maasakkers, Joannes D.; Borsdorff, Tobias; Landgraf, Jochen; Tol, Paul; van Kempen, Tim A.; van Hees, Richard; Hoogeveen, Ruud; Veefkind, J. Pepijn; Aben, Ilse

published in
Nature
2021

DOI (link to publisher)
10.1038/s41586-021-03712-y

document version
Publisher's PDF, also known as Version of record

Article

Vast CO_2 release from Australian fires in 2019–2020 constrained by satellite

https://doi.org/10.1038/s41586-021-03712-y

Received: 18 January 2021

Accepted: 7 June 2021

Published online: 15 September 2021

Check for updates

Ivar R. van der Velde[1,2]✉, Guido R. van der Werf[2], Sander Houweling[1,2], Joannes D. Maasakkers[1], Tobias Borsdorff[1], Jochen Landgraf[1], Paul Tol[1], Tim A. van Kempen[1], Richard van Hees[1], Ruud Hoogeveen[1], J. Pepijn Veefkind[3,4] & Ilse Aben[1,5]

Southeast Australia experienced intensive and geographically extensive wildfires during the 2019–2020 summer season[1,2]. The fires released substantial amounts of carbon dioxide into the atmosphere[3]. However, existing emission estimates based on fire inventories are uncertain[4], and vary by up to a factor of four for this event. Here we constrain emission estimates with the help of satellite observations of carbon monoxide[5], an analytical Bayesian inversion[6] and observed ratios between emitted carbon dioxide and carbon monoxide[7]. We estimate emissions of carbon dioxide to be 715 teragrams (range 517–867) from November 2019 to January 2020. This is more than twice the estimate derived by five different fire inventories[8–12], and broadly consistent with estimates based on a bottom-up bootstrap analysis of this fire episode[13]. Although fires occur regularly in the savannas in northern Australia, the recent episodes were extremely large in scale and intensity, burning unusually large areas of eucalyptus forest in the southeast[13]. The fires were driven partly by climate change[14,15], making better-constrained emission estimates particularly important. This is because the build-up of atmospheric carbon dioxide may become increasingly dependent on fire-driven climate–carbon feedbacks, as highlighted by this event[16].

On a global scale, emissions of carbon dioxide (CO_2) from wildfires are roughly equivalent to 22% of global fossil-fuel emissions[8]. Most of these fire-derived emissions are expected to be compensated for when vegetation regrows. This is not the case for fires burning in deforestation zones or peatlands, however, where carbon stocks are permanently reduced, adding to the build-up of atmospheric CO_2 over longer time scales. During the Southern Hemisphere summer of 2019–2020, about 74,000 km^2—an area roughly 2.5 times the area of Belgium—burned in the eucalyptus forests in the coastal region of Victoria and New South Wales in Australia[13]. The link with climate change and the expectation of a future with more frequent fires[15,16] suggests that part of the CO_2 emitted by these fires will not be sequestered by vegetation regrowth. Therefore, these fires will add to the build-up of atmospheric CO_2 over longer time scales and thus to climate change, which in turn promotes fire activity[16]. This class of fires is thus to some degree analogous to the aforementioned burning in deforestation zones or peatlands. Gaining a better understanding of the atmospheric burden of CO_2 these fires have caused (and will cause in the future) is therefore essential if we are to construct future scenarios of the global carbon balance. Here we use new high-quality carbon monoxide (CO) satellite measurements, in combination with other data, to derive CO_2 emissions for this extraordinary Southeast Australian wildfire episode.

Over the past few decades, advances in satellite technology, biogeochemical modelling and techniques to measure trace gases in the close vicinity of fires have resulted in a number of inventories of emissions from biomass burning[8–12]. These fire inventories combine satellite information on fire activity and area affected with information on land use or vegetation productivity to estimate spatially explicit fire emissions for a large number of trace gases and aerosols[17]. Although improvements have been made to increase the accuracy of such emission estimates, the uncertainties remain substantial, especially at regional scales[4,8]. For example, small fires or fires underneath the canopy or clouds go unnoticed, and several inventories rely on look-up tables of biome-averaged values, which inherently have a low spatial resolution[18].

For the Australian fire episode of 2019–2020, estimates of trace-gas emissions from five different fire inventory products diverge widely: for CO, for example, they range from 8.7 Tg to 36.1 Tg (Fig. 1). However, all inventories show that the CO emissions from wildfires of the 2019–2020 season in Southeast Australia were large, surpassing the biggest emissions of the previous 16 years by quite a margin. Indeed, approximately 70% of all CO released from Australian fires in November to January 2019–2020 came from the southeast, in contrast with an average contribution of 11% in previous years.

The underlying reasons for this large range of emission estimates include: differences in approach, especially the means of fire detection; variations in the parameterizations of fuel consumption used; and differences in the emission factors used to translate the rate of combustion of dry matter into actual emissions of trace gases[18]. We can split the inventories from which these estimates are derived into two categories: first, inventories based on burned area, namely the

[1]SRON Netherlands Institute for Space Research, Utrecht, The Netherlands. [2]Department of Earth Sciences, Vrije Universiteit, Amsterdam, The Netherlands. [3]Royal Netherlands Meteorological Institute (KNMI), De Bilt, The Netherlands. [4]Department of Geoscience and Remote Sensing, Delft University of Technology, Delft, The Netherlands. [5]Department of Physics and Astronomy, Vrije Universiteit, Amsterdam, The Netherlands. ✉e-mail: I.R.van.der.Velde@sron.nl

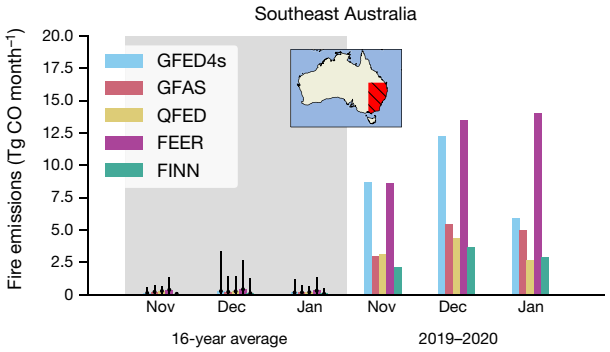

Fig. 1 | Comparison of fire emission estimates for Southeast Australia. CO emissions (in Tg CO month^{-1}) for the November to January 2019–2020 fire season in Southeast Australia (red highlighted region in inset), compared with the emission average of 16 previous years for the same period. Five different emission inventories are compared for each month: GFED4s, GFAS, QFED, FEER and FINN. Error bars represent the 16-year minimum and maximum values for each fire inventory.

Global Fire Emission Database version 4s (GFED4s; ref. [8]) and the Fire Inventory from NCAR version 1.5 (FINN[9]); and second, inventories based on fire radiative power (FRP), namely the Global Fire Assimilation System version 1.2 (GFAS[10]), Quick Fire Emissions Data set version 2.4 (QFED[11]), and Fire Energetics and Emission Research version 1.0 (FEER[12]). The burned-area-based inventories infer estimates of area burned from remotely sensed data in combination with a spatial and temporal representation of combustible biomass in the terrestrial biosphere[19]. The FRP-based inventories use the time integral of remotely sensed measurements of FRP, allowing for a more direct estimation of the rate of biomass combustion, and bypassing some of the uncertainties associated with the biogeochemical modelling that is needed in the burned-area approach[20]. However, FRP measurements introduce new challenges and uncertainties, including the translation of FRP into rates of biomass combustion[10]. Since 2016, the GFED4s inventory has been derived from a combination of the above strategies—it is no longer based on burned area and fuel consumption directly, but on FRP, scaled for each grid cell to emissions derived from burned area and fuel consumption for the overlapping 2003–2016 period[21] (see Supplementary Information).

Satellite measurements of trace gases throughout the entire atmospheric column have been shown to help curb the uncertainties in fire modelling and to provide more accurate estimates of CO_2 emission from fire[22,23]. Measurements of CO provide better top-down constraints than measurements of CO_2 itself, mostly because CO levels show a much larger (by up to several orders of magnitude) relative departure from background levels. These CO measurements, when combined with measurements of the CO_2:CO ratios in fire plumes, allow us to estimate CO_2 emissions from fire. For instance, different satellite data—including column measurements of CO—were used to constrain the 2015 Indonesia peat-fires, leading to emission estimates that are very different (either higher or lower, depending on the location) to those predicted by the fire inventories[22–26].

The launch of the TROPOspheric Monitoring Instrument (TROPOMI[5]) in October 2017 has provided new capabilities for CO observation. The instrument extends the capabilities of older legacy instruments by measuring the total column of CO at a much higher spatial resolution of 7 × 5.6 km^2, with daily global coverage. Under clear-sky conditions it also maintains high sensitivity up to the planetary boundary layer, where fire emissions have the largest impact. The instrument has been used previously to improve understanding of fires, their combustion characteristics and the atmospheric transport of emitted pollutants[27,28]. Here we use it in a regional inverse analysis to improve estimates of CO and CO_2 emission on a day-to-day basis for the Southeast Australian fires (see Supplementary Information).

Using this inverse analysis methodology, in combination with TROPOMI CO observations, we obtained improved (posterior) estimates of CO emission and simulated concentrations of regional CO that are more consistent with daily measurements than were the simulated CO amounts based on the (prior) inventory emissions alone. Figure 2a shows the prior November to January average CO mixing ratios from transport model simulations, with the GFAS fire emission inventory as input. Although the locations of wildfires and the resulting enhancement in CO are quite well captured by GFAS, the underestimation of CO relative to TROPOMI CO in Fig. 2b is evident. After optimization, the posterior CO mixing ratios in Fig. 2c become larger, yielding an 80% reduction in model–observation bias compared with the prior mixing ratios based on GFAS emissions. This is also the case for the other four inventories. The assessment of all five posterior estimates in the Taylor diagram[29] in Fig. 2d indicates a better match with observed CO in comparison with the priors. We obtained better correlation coefficients (11% higher on average), and larger spatial variability expressed as a standard deviation (84% increase on average). The small improvement in the correlation coefficient indicates that the general spatial pattern of enhancements in CO concentration is already captured well by the inventories before optimization. However, the reduction in root-mean-square-error (RMSE) and increase in variability indicate large adjustments in the absolute magnitude of emissions after optimization. Additional information and the results of inversions obtained using other fire inventories as priors can be found in the Supplementary Information.

Estimated CO emissions for the 2019–2020 fire episode are shown in Fig. 3 and Extended Data Table 1, for the five emission inventories (the priors) and our TROPOMI-constrained estimates (the posterior). In comparison with the prior estimates, we see in the posterior solutions a substantial enhancement of the monthly CO emissions that easily exceeds the variability among the ensemble of prior emission estimates (depicted by white circles, with $\pm 1\sigma$ variability). Our analysis also shows smaller differences between the posterior solutions than between the corresponding priors; the uncertainty among the ensemble of optimized emissions is reduced by more than 50% (black circles, with $\pm 1\sigma$ variability) in comparison with the prior ensemble uncertainty. This indicates that the posterior estimates are more robust than the priors and are more in agreement with the constraints imposed by atmospheric CO. The generally small differences between the posterior emission estimates stem from a persistent dependence on inventory emissions; this dependence, in addition to other factors such as transport and measurement uncertainty, prevents our inverse estimates from converging into an even more consistent solution.

As a next step, we calculated the amount of CO_2 emitted by these recent fires from the TROPOMI-inferred CO emissions in Fig. 3. This calculation was done using emission factors for CO_2 and CO determined from wildfires and prescribed burns in the southern Australian eucalyptus forests[7], summarized in Extended Data Table 3. The forested landscapes that burned in Southeast Australia were predominantly eucalyptus[30]. Biome-averaged data sets of emission factors that are often used in the fire emission inventories[17,31] are not detailed enough to describe fire emissions in Australia, where eucalyptus forests are part of the more general class of temperate forests[7]. Acquiring emission factors involves accurately measuring mixing ratios of trace gases or aerosols in the smoke plume using the carbon balance method[32]. These emission factors specify the mass of an aerosol or trace gas emitted per unit of dry matter burned, and, combined with the amount of biomass burned during a time interval, yield emission estimates for different chemical compounds[17]. We derived the average of the reported CO_2 and CO emission factors (EF_{CO2} and EF_{CO}) and their variability across the abovementioned literature (1,601 ± 40 g CO_2 kg^{-1} and 111 ± 14 g CO kg^{-1} dry matter, respectively) using different measurement

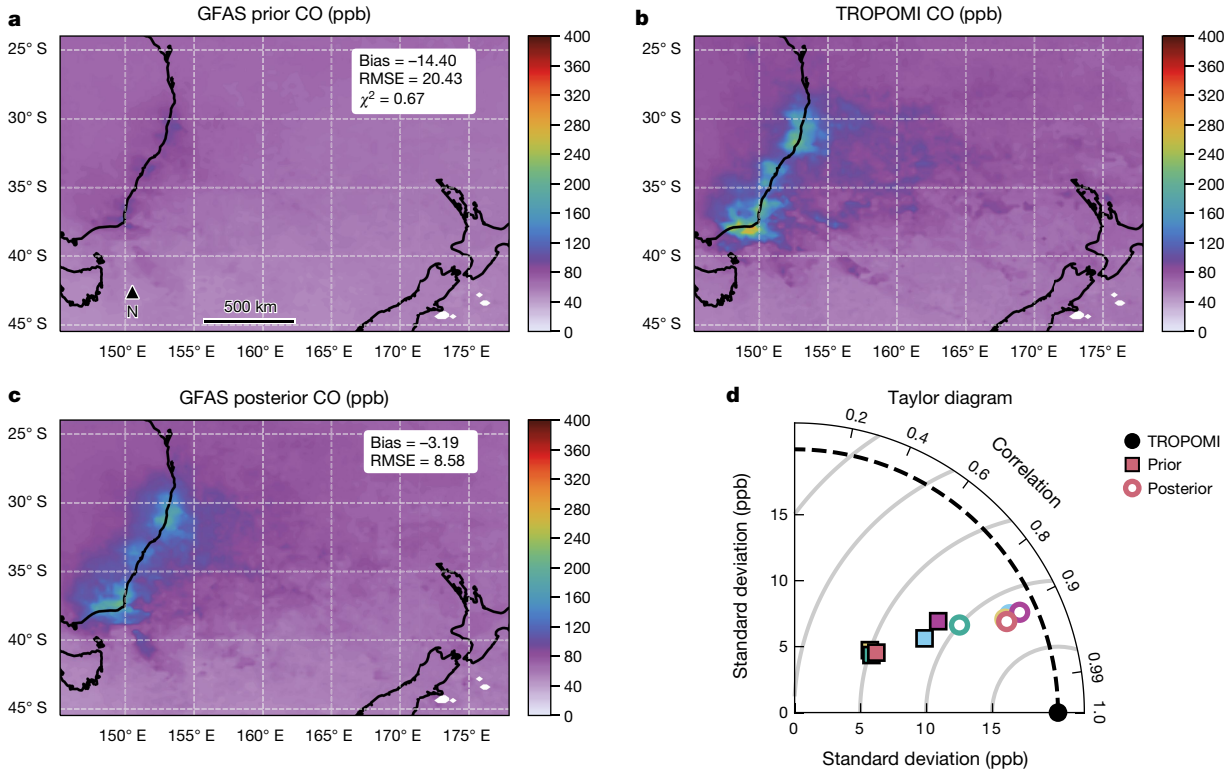

Fig. 2 | Comparison of simulated and observed CO column mixing ratios. Here, fire inventories are combined with TROPOMI information. **a**, Prior simulated CO column mixing ratios (in ppb), averaged for November to January 2019–2020, using the GFAS fire emissions as a boundary condition. **b**, TROPOMI-based average CO column mixing ratios for the same period. **c**, Improved posterior simulated mixing ratios for the same period. **d**, Verification of the inversion performance of all five inversions in a Taylor diagram. Shown is the correspondence between modelled (coloured symbols) and observed (black circle) CO mixing ratios, using the geometrical relationship of three statistics: Pearson's correlation coefficient (along the outer arc), centred RMSE (grey arcs) and the standard deviation (black dashed arc)[29]. The five prior estimates are shown with filled squares and the five posterior estimates with open circles, using the same colouring as Fig. 1. The posterior estimates lie closer to the dashed arc than do the prior estimates, indicating a larger standard deviation for the posterior estimates: that is, posterior variations in CO have an amplitude more similar to that of the TROPOMI data than do the prior variations. The posterior estimates also show a stronger correlation with the TROPOMI data and with the lower RMSE values. RMSE is indicated by the distance of the grey arcs from the black circle on the *x*-axis.

platforms (airborne and ground-based), for different types of burns (wildfires versus prescribed burns) and in different regions within our study domain. We then multiplied the CO emissions in Fig. 3 by the EF_{CO2}/EF_{CO} ratio (EFR = 14.4 ± 1.9 g CO_2/g CO) to obtain the estimates of CO_2 emission in Fig. 4.

Using the five posterior CO emission estimates and an EFR of 14.4 ± 1.9, we found emissions during the 2019–2020 fire episode to be 715 Tg CO_2. This is equivalent to 0.20 petagrams carbon (Pg C; 10^{15} g), or about 18% of the decadal averaged flux in global land-use change and land-cover change of 1.11 Pg C yr^{-1} (ref. [33]). A sensitivity analysis of our inversion framework showed that the real emission flux probably lies between 517 Tg and 867 Tg (based on a range of experiments; Extended Data Table 4). Our estimate is comparable to the 670 Tg CO_2 derived in a bottom-up bootstrap analysis of this fire episode[13]. As shown in Fig. 4 and Extended Data Table 2, these fires were large, even if you consider the lower limit of our estimate. Our new estimate is more than twice as large as the average of 275 Tg derived from the five fire inventories, and surpasses Australia's normal annual fire and fossil-fuel emissions by 80%.

A consequence of the infrequent nature of fires in eucalyptus forests in Southeast Australia is that the release of CO_2 is not in balance with the sequestration of carbon following previous fires on annual scales. Therefore, fires in these forests could potentially affect CO_2 growth rates more than savanna fires in northern and central Australia, where emissions and sequestration are more in balance[3]. Given the vastness of this event, the 2019–2020 fires may also increase CO_2 concentrations over the next few decades. Whether or not CO_2 concentrations are also affected on even longer time scales will depend on the degree to which increasing temperatures and more frequent drought episodes will influence future fire regimes in this region and thus the rate of

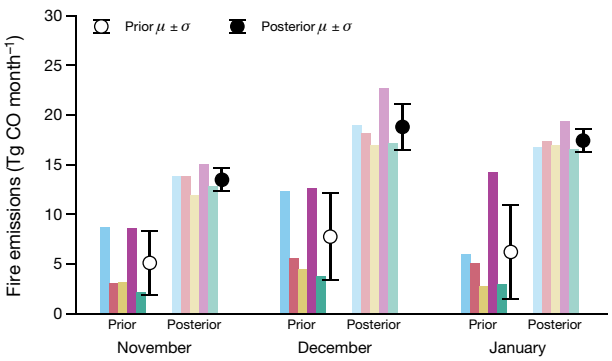

Fig. 3 | CO emissions from inventories and satellite constraints. Estimates of CO emission from fire (in Tg CO $month^{-1}$) for three consecutive months during the 2019–2020 Southeast Australian summer season. Darker bars show the five fire inventory estimates; lighter bars show estimates of posterior flux derived from the daily inversions (with colour coding as in Figs. 1, 2). Circles show monthly average estimates across the different inventories (white) and posterior results (black); error bars indicate the ±1σ variability across the five estimates. Extended Data Table 1 shows all emissions and uncertainties.

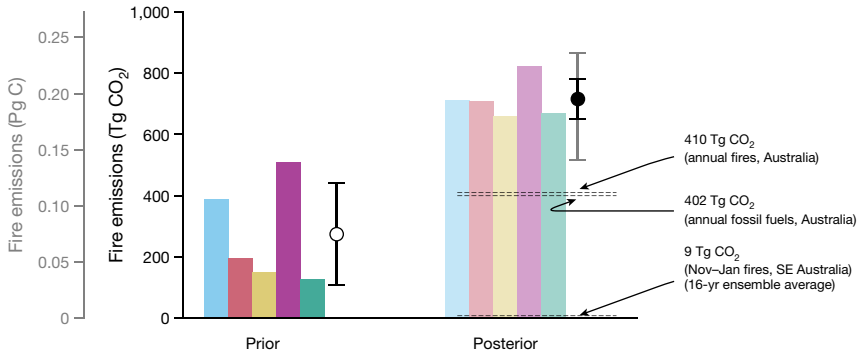

Fig. 4 | CO_2 emissions from inventories and satellite constraints. Shown are total estimates of CO_2 emission (in Tg CO_2 and Pg C) from fires for the Southeast Australian summer season of November to January 2019–2020. Darker bars show the five fire inventory estimates (the priors); lighter bars show posterior estimates derived from the inversions (with colour coding as in Figs. 1, 2). Extended Data Table 2 reports the values and uncertainties from all of the inversion estimates. Circles indicate three-month total estimates across the different fire inventories (white) and posterior results (black). The black error lines indicate the $\pm 1\sigma$ variability across the five inventories/inversion estimates. The grey error line indicates the minimum and maximum range in the posterior solutions, obtained using the different inversion options outlined in the Supplementary Information and Extended Data Table 4. To obtain a sense of scale, the three reference lines indicate Australia's normal wildfire and fossil-fuel emissions (upper dotted line, ref. [8]; centre dotted line, ref. [37]; lower dotted line, our data).

regrowth. All evidence points towards increases in the frequency of severe fire seasons in Southeast Australia[34–36], indicating that at least part of the emissions will not be offset in the future. From a climate perspective, these wildfires may therefore present a new category of fires that are neither CO_2 neutral nor fully net CO_2 emissions[8] but fall in between. Given the large magnitude of these events, as exemplified by our work, fire-driven climate-carbon feedbacks may become an increasingly relevant factor in determining future CO_2 levels.

Online content

Any methods, additional references, Nature Research reporting summaries, source data, extended data, supplementary information, acknowledgements, peer review information; details of author contributions and competing interests; and statements of data and code availability are available at https://doi.org/10.1038/s41586-021-03712-y.

1. Bowman, D. M. et al. Wildfires: Australia needs national monitoring agency. *Nature* **584**, 188–191 (2020).
2. Australian Government Annual Climate Statement 2019. http://www.bom.gov.au/climate/current/annual/aus/2019/ (last accessed 23 July 2021) (2019).
3. Australian Government Technical Update 2020. Estimating greenhouse gas emissions from bushfires in Australia's temperate forests: focus on 2019–20. https://www.industry.gov.au/sites/default/files/2020-04/estimating-greenhouse-gas-emissions-from-bushfires-in-australias-temperate-forests-focus-on-2019-20.pdf (last accessed 23 July 2021) (2020).
4. Pan, X. et al. Six global biomass burning emission datasets: intercomparison and application in one global aerosol model. *Atmos. Chem. Phys.* **20**, 969–994 (2020).
5. Veefkind, J. P. et al. TROPOMI on the ESA Sentinel-5 precursor: a GMES mission for global observations of the atmospheric composition for climate, air quality and ozone layer applications. *Remote Sens. Environ.* **120**, 70–83 (2012).
6. Tarantola, A. *Inverse Problem Theory and Methods for Model Parameter Estimation* (Soc. Indust. Appl. Math., Philadelphia, PA, 2005).
7. Guérette, E.-A. et al. Emissions of trace gases from Australian temperate forest fires: emission factors and dependence on modified combustion efficiency. *Atmos. Chem. Phys.* **18**, 3717–3735 (2018).
8. Van der Werf, G. R. et al. Global fire emissions estimates during 1997–2016. *Earth Syst. Sci. Data* **9**, 697–720 (2017).
9. Wiedinmyer, C. et al. The Fire Inventory from NCAR (FINN): a high resolution global model to estimate the emissions from open burning. *Geosci. Model Dev.* **4**, 625–641 (2011).
10. Kaiser, J. W. et al. Biomass burning emissions estimated with a global fire assimilation system based on observed fire radiative power. *Biogeosciences* **9**, 527–554 (2012).
11. Darmenov, A. & da Silva, A. The quick fire emissions dataset (QFED): documentation of versions 2.1, 2.2 and 2.4. *NASA Global Modeling and Assimilation Office* https://gmao.gsfc.nasa.gov/pubs/docs/Darmenov796.pdf (last accessed 23 July 2021) (2015).
12. Ichoku, C. & Ellison, L. Global top-down smoke-aerosol emissions estimation using satellite fire radiative power measurements. *Atmos. Chem. Phys.* **14**, 6643–6667 (2014).
13. Bowman, D. M. J. S., et al. Australian forests, megafires and the risk of dwindling carbon stocks. *Plant Cell Environ.* **44**, 347–355 (2021).
14. Van Oldenborgh, G. J. et al. Attribution of the Australian bushfire risk to anthropogenic climate change. *Nat. Hazards Earth Syst. Sci.* **21**, 941–960 (2021).
15. Abram, N. J. et al. Connections of climate change and variability to large and extreme forest fires in southeast Australia. *Commun. Earth Environ.* **2**, 8 (2021).
16. Shukla, P. R. et al. (eds). in *Climate Change and Land: an IPCC Special Report on Climate Change, Desertification, Land Degradation, Sustainable Land Management, Food Security, and Greenhouse Gas Fluxes in Terrestrial Ecosystems* (eds Shukla, P. R. et al.) (in the press).
17. Andreae, M. O. & Merlet, P. Emission of trace gases and aerosols from biomass burning. *Glob. Biogeochem. Cycles* **15**, 955–966 (2001).
18. Van Leeuwen, T. T. et al. Biomass burning fuel consumption rates: a field measurement database. *Biogeosciences* **11**, 7305–7329 (2014).
19. Seiler, W. & Crutzen, P. J. Estimates of gross and net fluxes of carbon between the biosphere and the atmosphere from biomass burning. *Clim. Change* **2**, 207–247 (1980).
20. Wooster, M. J. et al. Fire radiative energy for quantitative study of biomass burning: derivation from the BIRD experimental satellite and comparison to MODIS fire products. *Remote Sens. Environ.* **86**, 83–107 (2003).
21. Global Fire Emissions Database, version 4.1 (GFED4s): monthly and daily 1997–present. https://www.geo.vu.nl/~gwerf/GFED/GFED4/Readme.pdf (last accessed 23 July 2021)
22. Yin, Y. et al. Variability of fire carbon emissions in equatorial Asia and its nonlinear sensitivity to El Niño. *Geophys. Res. Lett.* **43**, 10472–10479 (2016).
23. Huijnen, V. et al. Fire carbon emissions over maritime Southeast Asia in 2015 largest since 1997. *Sci. Rep.* **6**, 26886 (2016).
24. Heymann, M. et al. CO2 emission of Indonesian fires in 2015 estimated from satellite-derived atmospheric CO2 concentrations. *Geophys. Res. Lett.* **44**, 1537–1544 (2017).
25. Lohberger, S. et al. Spatial evaluation of Indonesia's 2015 fire-affected area and estimated carbon emissions using Sentinel-1. *Glob. Change Biol.* **24**, 644–654 (2018).
26. Nechita-Banda, N. et al. Monitoring emissions from the 2015 Indonesian fires using CO satellite data. *Phil. Trans. R. Soc. Lond. B* **373**, 20170307 (2018).
27. Schneising, O. et al. Severe Californian wildfires in November 2018 observed from space: the carbon monoxide perspective. *Atmos. Chem. Phys* **20**, 3317–3332 (2020).
28. Van der Velde, I. R. et al. Biomass burning combustion efficiency observed from space using measurements of CO and NO_2 by the TROPOspheric Monitoring Instrument (TROPOMI). *Atmos. Chem. Phys.* **21**, 597–616 (2021).
29. Taylor, K. E. Summarizing multiple aspects of model performance in a single diagram. *J. Geophys. Res.* **106**, 7183–7192 (2001).
30. Wain, A. et al. Managing smoke from wildfires and prescribed burning in southern Australia. *Dev. Env. Sci.* **8**, 535–550 (2008).
31. Akagi, S. K. et al. Emission factors for open and domestic biomass burning for use in atmospheric models. *Atmos. Chem. Phys.* **11**, 4039–4072 (2011).
32. Yokelson, R. J. et al. Emissions of formaldehyde, acetic acid, methanol, and other trace gases from biomass fires in North Carolina measured by airborne Fourier transform infrared spectroscopy. *J. Geophys. Res.* **104** (D23), 30109–30125 (1999).
33. Houghton, R. A. & Nassikas, A. A. Global and regional fluxes of carbon from land use and land cover change 1850–2015. *Glob. Biogeochem. Cycles* **31**, 456–472 (2017).
34. Lucas, C. et al. *Bushfire weather in Southeast Australia: recent trends and projected climate change impacts*. Technical Report (Bushfire CRC and CSIRO Marine and Atmospheric Research, Melbourne, Australia, 2007).
35. Clarke, H. et al. Regional signatures of future fire weather over eastern Australia from global climate models. *Int. J. Wildland Fire* **20**, 550–562 (2011).
36. Matthews, S. et al. Climate change, fuel and fire behaviour in a eucalypt forest. *Glob. Change Biol.* **18**, 3212–3223 (2012).
37. Muntean, M. et al. *Fossil CO_2 Emissions of All World Countries: 2018 Report*. (European Commission JRC Science for Policy Report, 2018).

Data availability

TROPOMI measurements of CO can be downloaded from https://s5phub.copernicus.eu. GFED4s-based fire emissions can be downloaded from https://www.geo.vu.nl/~gwerf/GFED/GFED4/. GFAS-based fire emissions can be downloaded from https://apps.ecmwf.int/datasets/data/cams-gfas/. QFED-based fire emissions can be downloaded from https://portal.nccs.nasa.gov/datashare/iesa/aerosol/emissions/QFED/v2.5r1/0.1/QFED/. FEER-based fire emissions can be downloaded from https://feer.gsfc.nasa.gov/data/emissions/. FINN-based fire emissions can be downloaded from https://www.acom.ucar.edu/Data/fire/. Prior and posterior emissions and CO concentrations can be downloaded from https://doi.org/10.5281/zenodo.4692417.

Code availability

The Weather Research and Forecasting with Chemistry (WRF-CHEM) atmospheric transport model version 4.0 can be downloaded from https://www2.mmm.ucar.edu/wrf/users/download/get_source.html. Inversion and emission preparation codes are available at https://doi.org/10.5281/zenodo.4692678. Python notebooks used to create the figures and tables are at https://doi.org/10.5281/zenodo.5060184.

38. Hurst, D. F. et al. *Trace-Gas Emissions from Biomass Burning in Australia, in: Biomass Burning and Global Change*. (ed. Levine, J. S.) (MIT Press, 1996).
39. Lawson, S. J. et al. Biomass burning emissions of trace gases and particles in marine air at Cape Grim, Tasmania. *Atmos. Chem. Phys.* **15**, 13393–13411 (2015).
40. Paton-Walsh, C. et al. New emission factors for Australian vegetation fires measured using open-path Fourier transform infrared spectroscopy. Part 1. Methods and Australian temperate forest fires. *Atmos. Chem. Phys.* **14**, 11313–11333 (2014).
41. Rea, G. et al. Impact of the New South Wales fires during October 2013 on regional air quality in eastern Australia. *Atmos. Environ.* **131**, 150–163 (2016).
42. Reisen, F. et al. Ground-based field measurements of PM2.5 emission factors from flaming and smoldering combustion in eucalypt forests. *J. Geophys. Res.* **123**, 8301–8314 (2018).

Acknowledgements We thank the team that realized the TROPOMI instrument, comprising a partnership between Airbus Defence and Space Netherlands, the Royal Netherlands Meteorological Institute (KNMI), the SRON Netherlands Institute for Space Research and the Netherlands Organisation for Applied Scientific Research (TNO), commissioned by the Netherlands Space Office (NSO) and the European Space Agency (ESA). The Sentinel-5 Precursor is part of the European Union (EU) Copernicus programme, and Copernicus Sentinel data from 2019 and 2020 have been used here. The WRF model computations were carried out on the Dutch national e-infrastructure with the support of the SURF Cooperative. We also thank the large team of scientists and technicians who worked on the fire emission data sets available online. G.R.v.d.W. and I.R.v.d.V. are partly supported by the Netherlands Organization for Scientific Research (NWO; VICI research programme 016.160.324).

Author contributions I.R.v.d.V. analysed data, designed and ran the model simulations and wrote the paper. G.R.v.d.W., S.H. and I.A. provided scientific advice and detailed comments on the manuscript. J.D.M., T.B., T.A.v.K. and P.T. provided additional comments on the manuscript and TROPOMI products. J.L. and T.B. developed the TROPOMI CO product. R.v.H., T.A.v.K., P.T. and R.H. contributed to the TROPOMI shortwave-infrared (SWIR) calibration. J.P.V. is the principal investigator for the TROPOMI instrument.

Competing interests The authors declare no competing interests.

Additional information
Supplementary information The online version contains supplementary material available at https://doi.org/10.1038/s41586-021-03712-y.

Correspondence and requests for materials should be addressed to I.R.v.V.

Peer review information *Nature* thanks Johannes Kaiser and the other, anonymous, reviewer(s) for their contribution to the peer review of this work.

Extended Data Table 1 | Comparison of prior and posterior emissions of CO from fire for Southeast Australia

	Prior [Tg CO month^{-1}]			Posterior [Tg CO month^{-1}]		
	Nov	Dec	Jan	Nov	Dec	Jan
GFED4s	11.1±5.5 (8.7)	14.5±6.3 (12.3)	8.6±4.2 (5.9)	13.8±2.1	18.9±2.3	16.7±3.1
GFAS	5.5±2.1 (3.0)	7.9±2.6 (5.6)	7.7±4.1 (5.1)	13.8±2.3	18.1±2.6	17.3±3.6
QFED	5.6±1.7 (3.1)	6.7±1.6 (4.5)	5.3±1.3 (2.8)	11.9±3.0	17.0±2.8	17.0±4.7
FEER	10.9±5.3 (8.6)	14.8±3.7 (12.6)	16.8±13.3 (14.3)	15.0±2.2	22.7±2.6	19.4±3.5
FINN	4.6±1.1 (2.1)	6.0±1.4 (3.8)	5.6±1.5 (2.9)	12.8±2.2	17.2±2.5	16.6±3.5
Average	7.5±3.2 (5.1±3.2)	10.0±4.3 (7.8±4.4)	8.8±4.7 (6.2±4.7)	13.5±1.2	18.8±2.3	17.4±1.2

Comparison of the November to January 2019–2020 average prior and posterior CO fire emissions (in Tg CO month^{-1}) calculated for the five emission estimates over Southeast Australia. The monthly ± 1σ standard deviations are derived from the assumed error variances. The prior estimates in parentheses represent the inventory flux without the adjustment of zero emissions. The final row displays the model/inversion ensemble average and the ± 1σ standard deviation that depicts the variability across the five model estimates.

Extended Data Table 2 | Comparison of prior and posterior emissions of CO_2 from fire for Southeast Australia

	Prior [Tg CO_2] Nov–Jan	Posterior [Tg CO_2] Nov–Jan
GFED4s	491.5±150.0 (388.1)	713.3±113.5
GFAS	303.7±85.9 (196.9)	709.8±117.6
QFED	252.9±51.3 (150.3)	660.5±125.2
FEER	611.4±227.8 (510.4)	823.1±129.2
FINN	233.6±45.5 (127.2)	670.4±112.8
Average	378.6±165.4 (274.6±167.1)	715.4±64.6

Comparison of the November to January 2019–2020 average prior and posterior CO_2 fire emissions (in Tg CO_2) calculated from the five CO emissions estimates over Southeast Australia. The November to January ± 1σ standard deviations are derived from the assumed error variances and from the scaling uncertainty (in going from CO to CO_2 with an EFR of 14.4 ± 1.9; see equations (8) to (14) in the Supplementary Information). The prior estimates in parentheses represent the inventory flux with the EFR scaling but without the adjustment of zero emissions. The final row displays the model/inversion ensemble average and ± 1σ standard deviations that depict the variability across the five model estimates.

Extended Data Table 3 | Comparison of published CO_2 and CO emission factors and their ratios

	State	EF CO_2	EF CO	EFR	Platform	Type of fire
Hurst et al.[38] *	NSW	1577	99	15.9	Airborne	Wildfire
	NSW	1540	125	12.3	Airborne	Wildfire
	NSW	1558	104	15.0	Airborne	Wildfire
	NSW	1577	97	16.3	Airborne	Prescribed fire
Lawson et al.[39] *	TAS	1621	127	12.8	Ground-based	Wildfire
Paton-Walsh et al.[40] *	NSW	1620	118	13.7	Ground-based	Prescribed fire
Rea et al.[41] *	NSW	1640	107	15.3	Ground-based	Wildfire
Guérette et al.[7] *	VIC	1660	93	17.8	Ground-based	Prescribed fire
Reisen et al.[42] †	VIC	1612	127	12.7	Ground-based	Prescribed fire
Average		1601±40	111±14	14.4±1.9		

Comparison of the emission factors (EFs) for CO_2 and CO (in g kg^{-1} dry matter) reported in the literature[7,38–42]. The EF ratio (EFR) between CO_2 and CO is calculated for different locations in Southeast Australia (NSW, New South Wales; TAS, Tasmania; VIC, Victoria). The final row displays the average and the ± 1σ standard deviation of EFs and EFRs across all studies. The ± 1σ standard deviation of EFR is calculated using equation (9) in the Supplementary Information.

*Data sets from table 4 in ref. [7].

†Data based on an average across all flaming and smouldering samples.

Extended Data Table 4 | Overview of CO and CO_2 emission estimates for different experiments

Prior flux	Number of scaling parameters	Flux covariance structure	Posterior emissions [Tg CO]	Posterior emissions [Tg CO_2]	% negative emissions
GFED4s	20 flux parameters	300% diagonal-only uncertainty	42.0	604.8	7.0
GFED4s	20 flux parameters	covariance loc./300% uncertainty	42.4	610.6	5.8
GFED4s	20 flux parameters	covariance loc./100% uncertainty	40.2	580.3	2.9
GFED4s*	20 flux parameters	300% diagonal-only uncertainty	38.0	547.2	11.4
GFED4s	1 flux and 1 background parameter	300% diagonal-only uncertainty	35.9	517.0	0.0
GFED4s	20 flux and 1 background parameter	300% diagonal-only uncertainty	38.2	550.0	10.4
GFED4s†	**20 flux and 1 background parameter**	**300% diagonal-only uncertainty**	**49.5**	**713.3**	**30.4**
GFED4s†	1 flux and 1 background parameter	300% diagonal-only uncertainty	41.3	594.7	0.0
Flat prior	20 flux and 1 background parameter	300% diagonal-only uncertainty	60.2	866.9	34.8

Comparison of the November to January 2019–2020 posterior CO and CO_2 emission estimates (in Tg) for different experiments in which different flux and background scaling parameters were tested, in combination with different structures of the error covariance matrix *P*. The fraction of negative flux parameters (compared with the total parameters) is shown in the final column. The experiment in bold represents one of the five original estimates reported herein. The minimum and maximum CO_2 emission estimates (517.0 and 866.9 Tg CO_2) are incorporated into Fig. 4.

*Alternative background derived from CO concentration upwind of the fires.

†Prior flux adjustment everywhere fire inventory fluxes are zero.